Optimized Intermolecular Potential Functions for Amides and Peptides. Structure and Properties of Liquid Amides

William L. Jorgensen* and Carol J. Swenson

*Contribution from the Department of Chemistry, Purdue University,
West Lafayette, Indiana 47907. Received June 28, 1984*

Abstract: Optimized intermolecular potential functions have been determined for amides through Monte Carlo simulations of liquid formamide, *N*-methylacetamide (NMA), and dimethylformamide (DMF). The computed densities and heats of vaporization are within 2% of experimental values. In addition, the structural results are in excellent agreement with the available diffraction data for liquid formamide and DMF. Consistent with spectroscopic observations, liquid formamide and NMA feature winding hydrogen-bonded chains. A wide range of geometries is found for the hydrogen bonds, though cyclic hydrogen-bonded pairs are uncommon in liquid formamide. Local structure in liquid DMF is less striking; however, Coulombic interactions between neighbors are optimized, and there is a net favoring for antiparallel alignment of neighboring dipoles. The potential functions also provide reasonable energetic and geometrical descriptions of isolated amide dimers and amide–water complexes. The simplicity and proven utility of the functions make them particularly suitable for use in condensed-phase simulations of organic and biochemical systems.

The critical role of the aqueous environment in determining the structure and action of proteins necessitates the in-depth study of the hydration of small organic molecules, peptides, and biological macromolecules.[1] Progress is being made in this area through X-ray diffraction and NMR experiments[2] and through molecular dynamics and Monte Carlo statistical mechanics calculations. The theoretical methods are capable of providing particularly detailed descriptions of the structural, energetic, and dynamic characteristics of solute and solvent in aqueous solutions. Though computationally demanding, simulations have now been carried out for a variety of systems ranging from small polypeptides[3] to segments of DNA in water.[4] The interplay between theory and experiment in locating the localized water molecules in crystals of proteins and enzymes is also notable.[5-7] The potential for such studies is great, and extension to other important problems including enzyme–substrate binding and the origin of solvent effects on protein structure and dynamics is inevitable.

A key issue underlying the success of the simulation methods is the need for potential functions that properly describe the interatomic interactions in the modeled systems. Great effort has gone into the development of force fields for peptides.[8-13] However, the focus has often been on local conformational results, while the functions' abilities to represent intermolecular interactions have generally received only modest testing. The Hagler–Lifson[12] and EPEN/2[10] potentials are exceptions and involved parameterization with lattice constants and energies for amide crystals, though the latter are not well reproduced with EPEN/2.[10]

The development of water–peptide potential functions is less advanced. Aside from ad hoc combinations of available water and peptide potentials, two sets of functions represent a more systematic approach. The most widely used functions were developed by Clementi and co-workers from minimal basis set ab initio calculations on water–amino acid potential surfaces.[14] Such computations have well-known deficiencies in describing hydrogen bonding as well as dispersion interactions.[15] Furthermore, even if accurate two-body potentials could be obtained from high-quality ab initio calculations including electron correlation, the functions would have limited utility in fluid simulations due to the importance of many-body effects as is well-known for water.[16,17] Clementi's functions have received little critical evaluation in comparison to experimental data. The results from recent crystal water calculations are mixed and clouded by uncertainties concerning convergence of such computations and the amount of water in the samples.[6]

The other general water–peptide potentials are the EPEN/2 functions developed by Scheraga and co-workers.[10] These potentials have received little use in fluid simulations due in part to the large number of charged sites used to represent a molecule. This makes the evaluation of the potential functions very slow. The initial results for liquid water were also not very encouraging, and the poor performance on lattice energies for amides is of concern.[10]

In our work a different approach has been taken to generating intermolecular potential functions (IPFS). The aim is to develop well-tested IPFS that may be rapidly evaluated in fluid simulations and that yield thermodynamic and structural results for pure liquids and solutions in good agreement with experiment. Though a traditional emphasis has been on using crystal data in the parameterization of IPFS, our focus on fluid results is consistent with the primary targets of simulations which are liquids and solutions. The principal drawback of the approach is that it requires numerous fluid simulations to be carried out with trial sets of parameters. So far, optimized potentials for liquid simulations (OPLS functions) have been developed for water,[17] hydrogen fluoride,[18] the smaller alkali and halide ions,[19] and hydrocarbons.[20] The latter work was particularly extensive covering

(1) For a review, see: Nemethy, G.; Peer, W. J.; Scheraga, H. A. *Annu. Rev. Biophys. Bioeng.* **1981**, *10*, 459.

(2) For reviews, see: Matthews, B. W. *Annu. Rev. Phys. Chem.* **1976**, *27*, 493. Bryant, R. G. *Ibid.* **1978**, *29*, 167.

(3) Rossky, P. J.; Karplus, M. *J. Am. Chem. Soc.* **1979**, *101*, 1913. (b) Hagler, A. T.; Osguthorpe, D. J.; Robson, B. *Science (Washington, D. C.)* **1980**, *208*, 599.

(4) Corongiu, G.; Clementi, E. *Biopolymers* **1981**, *20*, 551; **1982**, *21*, 763.

(5) Hagler, A. T.; Moult, J. *Biopolymers* **1980**, *19*, 395; *Nature (London)* **1978**, *272*, 222.

(6) (a) Kim, K. S.; Corongiu, G.; Clementi, E. *J. Biomol. Struct. Dyn.* **1983**, *1*, 263. (b) Mezei, M.; Beveridge, D. L.; Berman, H. M.; Goodfellow, J. M.; Finney, J. L.; Neidle, S. *Ibid.* **1983**, *1*, 287.

(7) Hermans, J.; Vacatello, M. *ACS Symp. Ser.* **1980**, *No. 127*, 1.

(8) For a review, see: Levitt, M. *Annu. Rev. Biophys. Bioeng.* **1982**, *11*, 251.

(9) (a) Momany, F. A.; McQuire, R. F.; Burgess, A. W.; Scheraga, H. A. *J. Phys. Chem.* **1975**, *79*, 2361. (b) Dunfield, L. G.; Burgess, A. W.; Scheraga, H. A. *Ibid.* **1978**, *82*, 2609.

(10) (a) Nemenoff, R. A.; Snir, J.; Scheraga, H. A. *J. Phys. Chem.* **1978**, *82*, 2504. (b) Snir, J.; Nemenoff, R. A.; Scheraga, H. A. *Ibid.* **1978**, *82*, 2527.

(11) Gelin, B. R.; Karplus, M. *Biochemistry* **1979**, *18*, 1256.

(12) Hagler, A. T.; Huler, E.; Lifson, S. *J. Am. Chem. Soc.* **1974**, *96*, 5319. Hagler, A. T.; Lifson, S. *Ibid.* **1974**, *96*, 5327.

(13) Weiner, S. J.; Kollman, P. A.; Case, D. A.; Singh, U. C.; Ghio, C.; Alagona, G.; Profeta, S.; Weiner, P. *J. Am. Chem. Soc.* **1984**, *106*, 765.

(14) Clementi, E.; Cavallone, F.; Scordamaglia, R. *J. Am. Chem. Soc.* **1977**, *99*, 5531.

(15) (a) Dill, J. D.; Allen, L. C.; Topp, W. C.; Pople, J. A. *J. Am. Chem. Soc.* **1975**, *97*, 7220. (b) Jorgensen, W. L. *J. Chem. Phys.* **1979**, *71*, 5034.

(16) Jorgensen, W. L. *J. Chem. Phys.* **1981**, *75*, 2026.

(17) Jorgensen, W. L.; Chandrasekhar, J.; Madura, J. D.; Impey, R. W.; Klein, M. L. *J. Chem. Phys.* **1983**, *79*, 926.

(18) Cournoyer, M. E.; Jorgensen, W. L. *Mol. Phys.* **1984**, *51*, 119.

(19) Chandrasekhar, J.; Spellmeyer, D. C.; Jorgensen, W. L. *J. Am. Chem. Soc.* **1984**, *106*, 903.
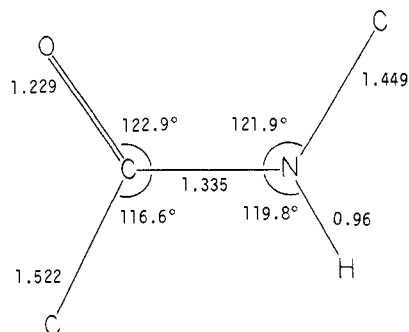
Figure 1. Standard geometry for amides and peptides taken from ref 25. Bond lengths in angstroms.

15 liquid alkanes, alkenes, and benzene, including all branching patterns for alkanes.[20] The accuracy of the OPLS functions is apparent in the average errors of 2% for the computed heats of vaporization and densities for the 17 pure liquids. The structural results also compare favorably with the available diffraction data on liquid water, hydrocarbons, and aqueous solutions of the ions.[17,19,20]

In the present work, the treatment has been extended to liquid amides. Specifically, OPLS parameters have been determined for the three classes of amides and tested in simulations of liquid formamide, *N*-methylacetamide (NMA), and dimethylformamide (DMF). The results also allow extensive characterization of the structure of these liquids which has been the topic of considerable discussion in the literature.[21-23] The parameterization for the amides involved careful analysis of the potential surfaces for amide-water complexes as well as amide dimers. Confirmation of the amide-water potential functions has been obtained through simulations of dilute aqueous solutions of the three amides as described in detail elsewhere.[24] It is important to note that in conjunction with the work on hydrocarbons,[20] OPLS functions now exist for describing the interactions between nine peptide residues (Ala, Val, Leu, Ile, Pro, Phe, Gly, Asn, and Gln) and between these residues and water. Parameters for terminal groups of polypeptides such as those incorporated in NMA are also provided. Work on the remaining peptide residues is progressing.

Computational Features

(a) Intermolecular Potential Functions. The IPFS are in the OPLS form in which molecules are represented by interaction sites usually located on the nuclei.[20] The interaction energy between two monomers a and b is then determined by Coulomb and Lennard-Jones interactions between all pairs of sites (eq 1).

$$\Delta\epsilon_{ab} = \sum_{i}^{on\ a} \sum_{j}^{on\ b} (q_i q_j e^2/r_{ij} + A_{ij}/r_{ij}^{12} - C_{ij}/r_{ij}^6) \qquad (1)$$

Standard combining rules are used such that $A_{ij} = (A_{ii}A_{jj})^{1/2}$ and $C_{ij} = (C_{ii}C_{jj})^{1/2}$. The A and C parameters may also be expressed

in terms of Lennard-Jones σ's and ϵ's as $A_{ii} = 4\epsilon_i\sigma_i^{12}$ and $C_{ii} = 4\epsilon_i\sigma_i^6$.

Some other important details are as follows. First, for computational efficiency, hydrogens on carbon are implicit while those on heteroatoms are explicitly represented.[20] Secondly, standard bond lengths and angles are used for the amides (and peptides) as summarized in Figure 1. The values are those recommended by Benedetti from his extensive analyses of crystal structures of polypeptides.[25] Torsional motion about the C-N bonds is considered in the next section. Finally, the interaction sites are located on the N, O, and H_N nuclei and on carbon for the CH_n groups. The potential function model is, therefore, the same as the 6-12 form used by Hagler, Huler, and Lifson except that they explicitly retain hydrogens on carbon.[12] We have tested their amide potentials and even run a simulation of liquid formamide with them as discussed below. For this purpose, the standard geometry (Figure 1) was employed augmented with a C_O-H bond length of 1.10 Å and NCH angle of 116.6°.

(b) Internal Rotation. Although the bond lengths and angles are fixed, rotation about the C_O-N bonds in the amides was included in the simulations. The local geometry about nitrogen and the carbonyl carbon was kept planar during the rotations; i.e., sp^2 hybridization was used for both atoms in all conformations. Incorporation of the torsion requires rotational potential functions to give the intramolecular energy as a function of the dihedral angle, ϕ.[26]

For formamide, NMR experiments and ab initio calculations concur that the barrier height is about 20 kcal/mol.[27] The twofold rotational potential can be well represented by eq 2 where $V_2 = 20$ kcal/mol.[27b]

$$V(\phi) = (V_2/2)(1 - \cos 2\phi) \qquad (2)$$

NMR data for NMA find the trans form (Figure 1) to be 2.8 kcal/mol lower in enthalpy than the cis isomer.[28,29] The trans-to-cis and cis-to-trans barrier heights were determined to be 22.6 and 19.8 kcal/mol and showed little solvent dependence.[28,30,31] These data have been incorporated into eq 3 which was used in

$$V(\phi) = (V_1/2)(1 - \cos\ \phi) + (V_2/2)(1 - \cos 2\phi) \qquad (3)$$

the simulations of liquid NMA with $V_1 = 2.8$ kcal/mol and $V_2 = 21.2$ kcal/mol. Thus, the trans form has $\phi = 0$ and the cis form has $\phi = \pi$.

NMR data are also available for DMF and yield barrier heights of about 20 kcal/mol in both the gas phase and solution.[31,32] Consequently, the rotational potential for formamide (eq 2) was appropriate for DMF as well.

(c) Monte Carlo Simulations. Statistical mechanics simulations were carried out for the three liquid amides with the OPLS functions and also with the Hagler-Lifson (H-L) potentials for formamide.[12] Standard procedures were employed including Metropolis sampling and periodic boundary conditions in the NPT ensemble.[26] Short simulations of ca. 500K configurations were used to optimize the OPLS parameters in addition to calculations on dimers and complexes discussed in the next section. Full simulations followed with the final parameter selections. These consisted of an equilibration phase of 500-1000K configurations with subsequent averaging over an additional 1000K configura-

(20) Jorgensen, W. L.; Madura, J. D.; Swenson, C. J. *J. Am. Chem. Soc.* **1984**, *106*, 6638.

(21) (a) Desando, R. J.; Brown, G. H. *J. Phys. Chem.* **1968**, *72*, 1088. (b) Itoh, K.; Shimanouchi, T. *J. Mol. Spectrosc.* **1972**, *42*, 86. (c) Siegbahn, H.; Asplund, L.; Kelfve, P.; Hamrin, K.; Karlsson, L.; Siegbahn, K. *J. Electron. Spectrosc. Relat. Phenom.* **1974**, *5*, 1059. (d) Pullman, A.; Berthod, H.; Giessner-Prettre, C.; Hinton, J. F.; Harpool, D. *J. Am. Chem. Soc.* **1978**, *100*, 3991. (e) Nielsen, O. F.; Lund, P.-A.; Praestgaard, E. *J. Chem. Phys.* **1982**, *77*, 3878. (f) Ohtaki, H.; Funaki, A.; Rode, B. M.; Reibnegger, G. J. *Bull. Chem. Soc. Jpn.* **1983**, *56*, 2116. (g) Kalman, E.; Serke, I.; Palinkas, G.; Zeidler, M. D.; Wiesmann, F. J.; Bertagnolli, H.; Chieux, P. *Z. Naturforsch., A* **1983**, *38A*, 231.

(22) (a) Mizushima, S.; Simanouti, T.; Nagakura, S.; Kuratani, K.; Tsuboi, M.; Baba, H.; Fujioka, O. *J. Am. Chem. Soc.* **1950**, *72*, 3490. (b) Lin, R.; Dannhauser, W. *J. Phys. Chem.* **1963**, *67*, 1805. (c) McLachlan, R. D.; Nyquist, R. A. *Spectrochim. Acta* **1964**, *20*, 1397. (d) Furer, A. L.; Zhikhareva, N. A.; Marlahov, L. I. *Zh. Priklad. Spektros.* **1981**, *34*, 872.

(23) (a) Whittaker, A. G.; Siegel, S. *J. Chem. Phys.* **1965**, *42*, 3320. (b) Fini, G.; Mirone, P. *J. Chem. Soc., Faraday Trans. 2* **1974**, *70*, 1776. (c) Ohtaki, H.; Itoh, S.; Yamaguchi, T.; Ishiguro, S.; Rode, B. M. *Bull. Chem. Soc. Jpn.* **1983**, *56*, 3406.

(24) Jorgensen, W. L.; Swenson, C. J. *J. Am. Chem. Soc.*, in press.

(25) Benedetti, E. In "Proceedings of the Fifth American Peptide Symposium"; Goodman, M., Meienhofer, J.; Eds.; Wiley: New York, 1977; p 257.

(26) For a review, see: Jorgensen, W. L. *J. Phys. Chem.* **1983**, *87*, 5304.

(27) (a) Drakenberg, T.; Forsen, S. *J. Phys. Chem.* **1970**, *74*, 1. (b) Perricaudet, M.; Pullman, A. *Int. J. Peptide Protein Res.* **1973**, *5*, 99.

(28) Drakenberg, T.; Forsen, S. *J. Chem. Soc., Chem. Commun.* **1971**, 1404.

(29) Barker, R. H.; Boudreaux, G. J. *Spectrochim. Acta, Part A* **1967**, *23A*, 727.

(30) Neuman, R. C.; Jonas, V.; Anderson, K.; Barry, R. *Biochem. Biophys. Res. Commun.* **1971**, *44*, 1156.

(31) Drakenberg, T.; Dahlqvist, K.-I.; Forsen, S. *J. Phys. Chem.* **1972**, *76*, 2178.

(32) Ross, B. D.; True, N. S. *J. Am. Chem. Soc.* **1984**, *106*, 2451.

Potential Functions for Amides and Peptides

J. Am. Chem. Soc., Vol. 107, No. 3, 1985 571

tions. The simulation of formamide with the H–L potential was actually carried out first and consisted of a 500K equilibration and averaging over 1500K. Starting configurations were obtained by modifying configurations from the simulations of hydrocarbons with similar molecular volumes.[20]

Each system consisted of 128 monomers in a cubic cell. The external pressure was fixed at 1 atm, and the simulations were run at temperatures of 25 °C for formamide and 100 °C for NMA and DMF. The higher temperature for NMA was desirable due to its higher melting point (31 °C) and the greater availability of thermodynamic data for the liquid at 100 °C than at 25 °C.[33] The melting points for formamide and DMF are 3 and –61 °C. Subsequently, a simulation of liquid DMF was also run at 25 °C as discussed in the Note Added in Proof.[47]

Spherical cutoffs were used to truncate the intermolecular interactions at distances of 10 Å for formamide and 12 Å for NMA and DMF. Therefore, interactions with a molecule's 50–60 nearest neighbors were evaluated explicitly. A correction was made to the energy during the simulations only for the Lennard-Jones interactions neglected beyond the cutoff. This was accomplished in the usual manner[20] and accounted for about 2% of the total energies. The cutoff was based on roughly the center-of-mass separations. Procedures for making cutoff corrections for the Coulombic interactions are not as straightforward or well established.[34] They are often not made for dipolar liquids and may be anticipated to have little effect on the present results.[34]

The ranges for the translations and rotations of the monomers and for the volume changes were adjusted to yield overall acceptance probabilities of ca. 40% for new configurations. The internal rotation for a monomer was also attempted on each move within ranges of ±12°. For lower rotational barriers, we normally use umbrella sampling methods to enhance conformational transitions.[26] This is not necessary and was not employed for formamide and DMF owing to the symmetry of $V(\phi)$ in these cases. It was also not employed for NMA, though the cis and trans forms are not equivalent. This decision is reasonable since the chosen $V(\phi)$ (eq 3) is based on liquid data and due to the limited medium sensitivity observed for the rotational potentials of amides.[28-32] However, 3 of the 128 NMA monomers were started out cis and stayed that way throughout the simulation to be consistent with the Boltzmann distribution for $V(\phi)$. The other 125 monomers remained trans.

The computations were executed on a Harris Corp. H-80 computer in our laboratory.

Results and Discussion

(a) Optimization of OPLS Parameters and Results for Dimers. The q, A, and C parameters for the intermolecular potential functions were optimized through a series of Monte Carlo simulations on the three liquids and simultaneous analyses of interaction energies and geometries for amide dimers and amide–water complexes. The chief points of comparison with experiment in the liquid simulations were for densities, heats of vaporization, and locations and areas of peaks in the radial distribution functions for formamide and DMF. The final parameter values are summarized in Table I. Effort was made to minimize the number of atom types and to maintain consistency with the parameters for hydrocarbons.[20] Other convenient and advantageous features were incorporated as summarized below.

(1) It was possible to use the same ϵ and σ for nitrogen in primary, secondary, and tertiary amides and the same charge for nitrogen in the latter two cases. Thus, all nitrogens in peptide backbones are identical. (2) As in the H–L potentials,[12] the Lennard-Jones parameters for hydrogens on heteroatoms may be taken as zero. (3) The carbonyl and NH_2, NHR, and NRR'

Table I. OPLS Parameters for Amides, Peptides, and Water

atom or group	example	q	σ, Å	ϵ, kcal/mol
N (1°)	formamide, Asn	−0.85	3.25	0.170
N (2°)	NMA, Ala	−0.57	3.25	0.170
N (3°)	DMF, Pro	−0.57	3.25	0.170
H (N1°)	formamide, Asn	0.425	0.0	0.0
H (N2°)	NMA, Ala	0.37	0.0	0.0
O (C=O)	amides	−0.50	2.96	0.210
C (C=O)	NMA, Ala	0.50	3.75	0.105
CH (CH=O)	formamide	0.50	3.80	0.115
CH₃ (N2°)	NMA	0.20	3.80	0.170
CH₃ (N3°)	DMF	0.285	3.80	0.170
CH₂ (N2°)	C_α in Gly	0.20	3.80	0.118
CH (N2°)	C_α in Ala	0.20	3.80	0.080
CH (N3°)	C_α in Pro	0.285	3.80	0.080
CH₂ (N3°)	Pro	0.285	3.80	0.118
CH₃ (C=O)	NMA	0.0	3.91	0.160
O (H₂O)	water	0.0	3.1536	0.15504
H (H₂O)	water	0.52	0.0	0.0
M (H₂O)[a]	water	−1.04	0.0	0.0

[a] M is a point on the HOH bisector, 0.15 Å from oxygen toward the hydrogens.
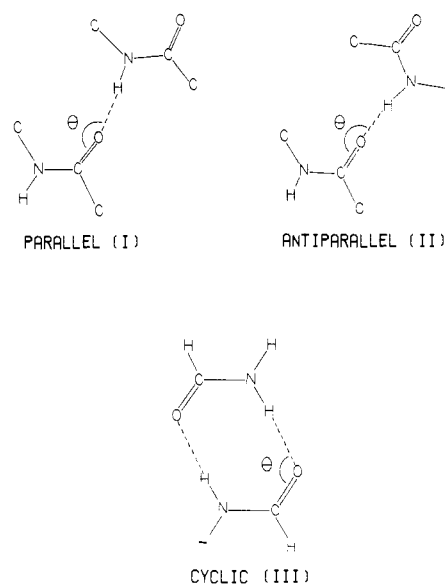

Figure 2. Geometrical arrangements for amide dimers.

groups are separately neutral. (4) The pattern of charges is qualitatively similar to the H–L potentials, though larger in magnitude, and consistent with population analyses from ab initio calculations.[12] (5) The ϵ and σ for carbonyl C and CH are the same as for C and CH in alkenes.[20] However, it was necessary to use slightly smaller ϵ's and σ's for CH₃ groups on nitrogen than for the same groups in alkanes.[20] Consistent parameters for CH₂ and CH groups on amide nitrogen are also provided in Table I, though they have not been tested. These groups are relatively buried in peptides, and the precise choice of Lennard-Jones parameters should not be critical within reasonable limits. However, the charges are fixed by the charges determined for nitrogen and the neutrality condition. (6) The charge on C_α in peptides is 0.20 for secondary residues and 0.285 for proline. These values are consistent with other peptide IPFS.[12,13] In the OPLS formalism, the side chains in peptides are to be separately charge balanced, i.e., neutral or with net charges of ±1. For purely hydrocarbon side chains, each CH$_n$ groups is uncharged.[20] Several of the above features make the OPLS functions particularly convenient for simulations of biochemical systems.

(7) The charge distributions yield dipole moments of 4.33, 4.23, and 4.45 D for formamide, NMA, and DMF, respectively. The corresponding experimental gas-phase values are 3.7, 3.7, and 3.9 D.[34] This fits a pattern that we have found: point charge distributions need to yield dipole moments about 15% greater than gas-phase values in potential functions designed for liquid simu-

(33) (a) Lemire, R. J.; Sears, P. G. *Top. Curr. Chem.* **1978**, *74*, 45. (b) Covington, A. K.; Dickinson, T. "Physical Chemistry of Organic Solvent Systems"; Plenum: London, 1973; Chapter 1.

(34) Klein, M. L.; McDonald, I. R.; Berne, B. J.; Rao, M.; Beveridge, D. L.; Mehrotra, P. K. *J. Chem. Phys.* **1979**, *71*, 3889. Pangali, C.; Rao, M.; Berne, B. J. *Mol. Phys.* **1980**, *40*, 661. Impey, R. W.; Madden, P. A.; McDonald, I. R. *Ibid.* **1982**, *46*, 513.

Table II. Geometries and Interaction Energies (kcal/mol) for Amide Dimers

dimer	potential	r_{NO}, Å	θ, deg	$-\Delta E$
formamide (I)	H–L	2.91	189	5.73
formamide (II)	H–L	2.91	162	5.83
formamide (III)	H–L	2.94	117	10.25
formamide (I)	OPLS	2.78	194	7.96
formamide (II)	OPLS	2.77	170	8.13
formamide (III)	OPLS	2.81	119	14.07
NMA (I)	H–L	2.95	154	6.25
NMA (II)	H–L	2.94	174	6.16
NMA (I)	OPLS	2.79	166	8.91
NMA (II)	OPLS	2.79	184	8.97
DMF (I)	OPLS	4.74	189	2.97
DMF (II)	OPLS	4.72	156	3.12
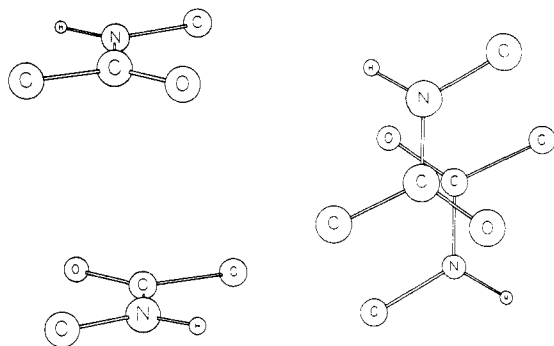
Figure 3. Two views of a stacked dimer for NMA. The dimerization energy from the OPLS functions is –5.6 kcal/mol.

lations.[17,18] (8) The TIP4P parameters for water[17] are included in Table I and taken as part of the OPLS set. The simpler TIP3P potential would also be adequate for most purposes.[17] The parameters for hydrocarbon groups are summarized elsewhere.[20]

Geometry optimizations were carried out for a variety of structures for amide dimers. The three hydrogen-bonded forms found in solid formamide are illustrated in Figure 2.[35] The antiparallel structure (II) also provides the hydrogen bonding in crystalline NMA.[36] The results of optimizations for these structures with the OPLS and H–L potentials are provided in Table II.

There are many qualitative similarities in the two sets of results for formamide and NMA dimers. For example, the hydrogen bonds are a little longer and stronger for NMA than formamide in structures I and II. The angular results are similar for all forms. Furthermore, the cyclic formamide dimers are bound by somewhat less than twice the energy of two acyclic hydrogen bonds. Consistently, the hydrogen bond lengths are longer in the cyclic structure than in forms I and II. This is also true in the solid where the X-ray results at –50 °C find the two NO distances to be 2.935 and 2.88 Å.[35] The hydrogen bond length in crystalline NMA at –35 °C is somewhat shorter (2.825 Å) and closer to the OPLS value for the dimers.[36] The principal differences between the H–L and OPLS results are that the optimum hydrogen bonds are ca. 0.15 Å shorter and 2–3 kcal/mol stronger with the OPLS functions. As shown below, these features are desirable as the H–L potential yields an energy and density for liquid formamide that are too high and a little low, respectively.

Results for DMF dimers in structures analogous to I and II are also given in Table II for the OPLS function. Since hydrogen bonding is not possible, general dipole–dipole attraction is operative. These are not the lowest energy forms for DMF dimers; stacked alternatives with antiparallel dipoles yield interaction energies as low as –6 kcal/mol. Stacked dimers were also investigated for formamide and NMA. For formamide, the stacked forms collapse to the cyclic structure (III) or a stacked version of it, if the monomers are forced to remain in parallel planes,

Table III. Volumes and Densities for Liquid Amides

	formamide		NMA	DMF
	H–L	OPLS		
T, °C	25	25	100	100
V, Å³	69.6	66.8	141.3	138.0
V (exptl)	66.3[a]	66.3[a]	135.9[b]	139.0[c]
d, g cm⁻³	1.075	1.120	0.859	0.879
d (exptl)	1.129[a]	1.129[a]	0.894[b]	0.873[c]

[a] Reference 33b. [b] Reference 33a. [c] References 38 and 39.

Table IV. Energetic Results for Liquid Amides[a]

	formamide		NMA	DMF
	H–L	OPLS		
T, °C	25	25	100	100
$-E_i(l)$	12.21	14.20	12.44	9.75
$E_{intra}(l)$	0.31	0.31	0.45	0.38
$E_{intra}(g)$	0.30	0.30	0.44	0.38
ΔE_{vap}	12.20	14.19	12.43	9.75
ΔH_{vap}	12.79	14.78	13.17	10.49
ΔH_{vap}(exptl)	14.7[b]	14.7[b]	13.3[c]	10.4[d]
$C°_P$(ig)	11.1[e]	11.1[e]	24.8[e]	25.4[e]
$C_P(l)$	22.9	19.2	40.4	33.5
$C_P(l)$(exptl)	25.7[f]	25.7[f]		38.7[d]

[a] Energies and enthalpies in kcal/mol, heat capacities in cal/mol K. [b] Reference 40. [c] Reference 33a. [d] Reference 41. [e] Reference 42. [f] Reference 43.

during the optimizations. For NMA, two stacked dimers with interplane separations of ca. 3.6 Å and interaction energies of –5.3 and –5.6 kcal/mol were optimized. Both feature antiparallel dipole alignment with maximization of O–H_N and C_O–N attractions; two views of the lower energy structure are shown in Figure 3.

Besides these considerations, the potential functions were chosen to yield reasonable results for amide–water complexes. Though the details will be presented subsequently,[24] a few points should be noted. We have performed ab initio calculations with the 6-31G* basis set on 3-21G optimized geometries for the four hydrogen-bonded forms of formamide–water previously studied by Alagona et al. with smaller basis sets.[37] These calculations show that the carbonyl oxygen is a better hydrogen bond acceptor than the NH group is a donor by about 1 kcal/mol. The OPLS parameters were chosen to maintain this trend and provide reasonable water–amide interaction energies and geometries. The optimum water–NMA hydrogen bond at the carbonyl group has a strength of 7.4 kcal/mol and an OO separation of 2.72 Å. The corresponding values for the linear water dimer with the TIP4P potential are 6.2 kcal/mol and 2.75 Å. Thus, the hydrogen bonds get stronger along the series water–water, water–amide, amide–amide.

In summary, it has been established that the OPLS functions provide a reasonable and internally consistent representation of hydrogen bonding involving amides and water. More decisive tests are embodied in the fluid simulations.

(b) Thermodynamics. The thermodynamic results from the full liquid simulations with the final parameters are recorded in Tables III and IV. The computed volumes and densities are compared with experimental values in Table III. The average statistical uncertainty ($\pm 1\sigma$) in the computed quantities is ± 0.2 Å³ and ± 0.001 g cm⁻³. These estimates were obtained from fluctuations in the averages for blocks of 50K configurations. The average error in comparison with experimental densities for the OPLS results is 1.7%. The Hagler–Lifson potential also fares quite well for formamide, yielding an error of 5.0%. The larger molecular

(35) Ladell, J.; Post, B. *Acta Crystallogr.* **1954**, *7*, 559.
(36) Katz, L. J.; Post, B. *Acta Crystallogr.* **1960**, *13*, 624.

(37) Alagona, G.; Pullman, A.; Scrocco, E.; Tomasi, J. *Int. J. Peptide Protein Res.* **1973**, *5*, 251.
(38) Gopal, R.; Rizgi, S. A. *J. Ind. Chem. Soc.* **1966**, *43*, 179. Geller, B. E. *Zh. Fiz. Khim.* **1961**, *35*, 2210.
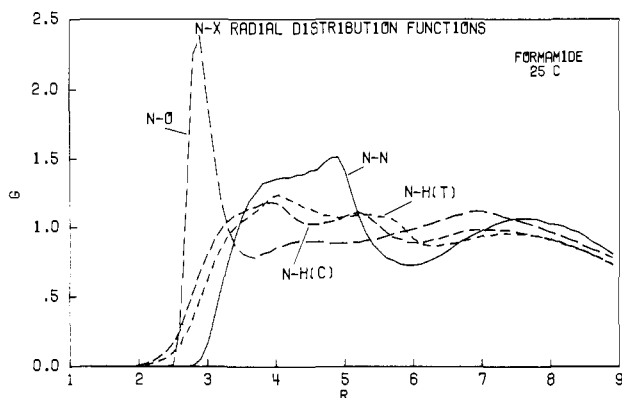(39) Zegers, H. C.; Somsen, G. *J. Chem. Thermodyn.* **1984**, *16*, 225.
(40) Somsen, G.; Coops, J. *Rec. Trav. Chim.* **1965**, *84*, 985.
(41) "DMF Product Bulletin"; E. I. duPont, Inc.: Wilmington, DE, 1971.
(42) Benson, S. W. "Thermochemical Kinetics"; Wiley: New York, 1976.
(43) Skold, R.; Suurkuusk, J.; Wadso, I. *J. Chem. Thermodyn.* **1976**, *8*, 1075.

Potential Functions for Amides and Peptides

J. Am. Chem. Soc., Vol. 107, No. 3, 1985 573

Figure 4. Rdfs for liquid formamide computed with the OPLS functions. H(C) and H(T) are the hydrogens cis and trans to the oxygen. Distances on the *x* axis are in angstroms throughout.

volume is consistent with the longer optimal hydrogen bonds with the H–L potential (Table II). It should be emphasized that this analysis is simplistic since the full potential surface affects the computed properties due to the thermal, configurational averaging. The unit cell volume was also slightly overestimated in the crystal calculations for formamide by Hagler et al.[12] The volume and error would increase further in their computations if thermal averaging was included.

The computed energetic results are presented in Table IV and compared with experimental heats of vaporization and heat capacities. The heat of vaporization is computed via eq 4 where E_i is the total intermolecular energy for the liquid. E_i is computed

$$\Delta H_{vap} = E_{intra}(g) - (E_i(l) + E_{intra}(l)) + RT \qquad (4)$$

from the pairwise sum over all of the intermolecular interaction energies plus the cutoff correction.[20,26] The intramolecular rotational energy for the ideal gas, $E_{intra}(g)$, is obtained from a Boltzmann distribution for $V(\phi)$ while the value for the liquid is determined by averaging the total intramolecular rotational energy during the simulations. The computed heat capacities, $C_P(l)$, are estimated from the fluctuation in the intermolecular energy plus a unimolecular term taken as the heat capacity of the ideal gas less R (to subtract out the PV term for the ideal gas).

The computed heats of vaporization with the OPLS potentials reproduce the experimental data; the average error is 0.8% which is within the uncertainty in the experimental values. The statistical uncertainty in the computed data is ca. ±0.025 kcal/mol. The H–L results for ΔH_{vap} of formamide underestimate the observed value by 13%. The lattice energy for solid formamide was also underestimated; the 6% discrepancy is again anticipated to increase if thermal averaging is allowed.[12]

The computed heat capacities converge relatively slowly. The reported values in Table IV may underestimate the true results for these potential functions by as much as 5 eu.[44] Therefore, the low computed values in Table IV are not unreasonable. The isothermal compressibility (κ) and coefficient of thermal expansion (α) were also computed from the standard fluctuation formulas. However, these quantities converge so slowly that they have no diagnostic value. The computed values have the right order of magnitude but fluctuate significantly.[44]

One final point should be noted from the data in Table IV. There is no change in the intramolecular rotational energy and in the distribution functions for the dihedral angles for these systems upon passing from the gas phase to the liquid. This is consistent with the modest sensitivity of the barrier heights to solvent variation.[28–32] It is also reasonable since there is no change in dipole moments for formamide and DMF and little change for NMA as a function of conformation using the OPLS charge distributions.[26]

(c) Radial Distribution Functions. Formamide. The radial distribution functions (rdfs) computed for liquid formamide with

(44) Jorgensen, W. L. *Chem. Phys. Lett.* **1982**, *92*, 405.
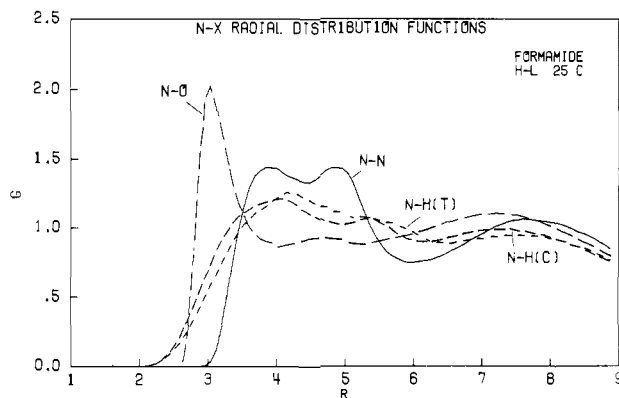
Figure 5. Same rdfs as in Figure 4 but computed with the Hagler–Lifson potentials.
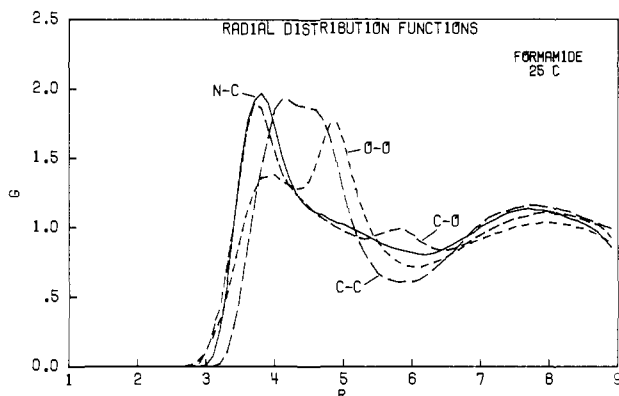
Figure 6. Rdfs for liquid formamide computed with the OPLS functions.

the OPLS functions are shown in Figures 4, 6, and 7. H(C) and H(T) in these figures refer to the hydrogens on nitrogen that are cis or trans to oxygen. For comparison, Figure 5 contains the same rdfs as Figure 4 but computed with the H–L potential. The corresponding rdfs from both potential functions are all qualitatively the same. Quantitatively, the stronger hydrogen bonding with the OPLS functions is reflected primarily in higher and sharper first peaks for the N–O, O–H(C), and O–H(T) rdfs. However, it is clear that both potential functions yield fundamentally the same structure for liquid formamide.

Hydrogen bonding is responsible for the striking first peak in the N–O rdf (Figure 4) which has its maximum at 2.9 Å. Integration of the peak to the minimum at 3.7 Å yields 2.7 contacts or an average of 5.4 neighbors per monomer within this range. The peak position has also been determined from a recent, combined study using X-ray, neutron, and electron diffraction on liquid formamide at 25 °C.[21g] The experimental finding is also 2.9 Å.[21g] It should be noted that two other X-ray studies on the liquid found the peak at 3.05 Å which coincides with the prediction from the H–L potential (Figure 5).[21a,f] Unfortunately, the full individual rdfs are not yet available from the diffraction experiments; the principal experimental data are for a few peak positions. In particular, the peaks in the X-ray results at 3.75 and 5.0 Å must be assigned to a combination of bands from individual atom–atom rdfs including the N–N (Figure 4) and N–C, C–C, C–O, and O–O (Figure 6).[21a]

The only other intermolecular peak assigned from the diffraction experiments is for O–H contacts at 1.9 Å.[21g] Again perfect accord is obtained with the calculated position of the first O–H peaks in Figure 7. Some insights into details of the hydrogen bonding are provided in this figure, though more extensive analyses are presented below. First, both the cis and trans hydrogens are participating in hydrogen bonds to roughly equal extents; the first peaks out to 2.8 Å integrate to 0.97 and 1.05 contacts for H(C) and H(T), respectively. This rules out a predominance of cyclic dimers in the liquid. It also implies that each monomer might participate in roughly four hydrogen bonds which agrees with the estimate from the diffraction experiments.[21g] In reality, the data
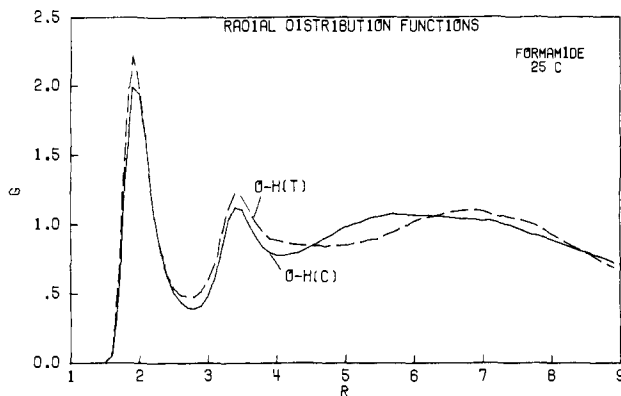
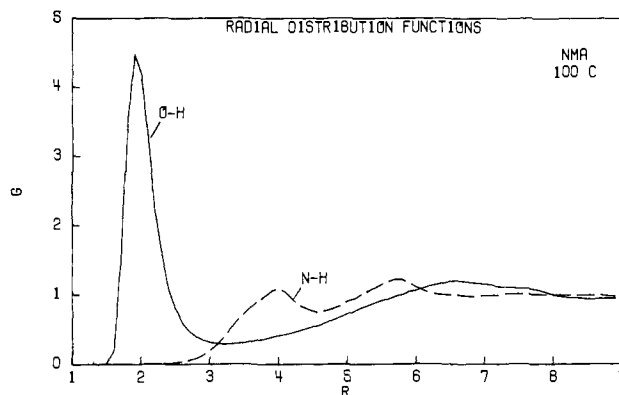**Figure 7.** O–H rdfs for liquid formamide computed with the OPLS functions.

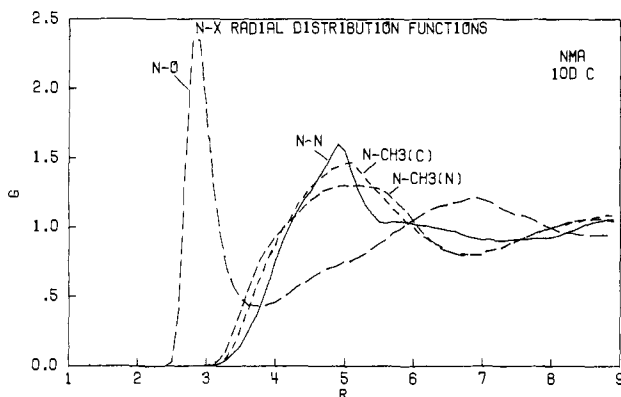**Figure 8.** Rdfs for liquid NMA computed with the OPLS functions.

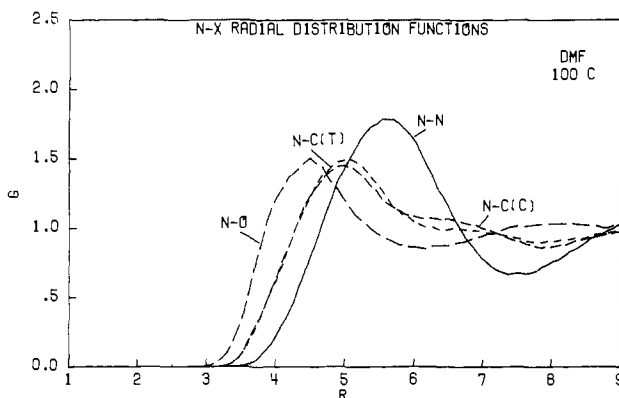**Figure 9.** Rdfs for liquid NMA computed with the OPLS functions. CH3(N) and CH3(C) are the methyl groups on nitrogen and carbonyl carbon.

Figure 10. O–H and N–H rdfs for liquid NMA computed with the OPLS functions.

Figure 11. Rdfs for liquid DMF computed with the OPLS functions. C(C) and C(T) are the methyl carbons cis and trans to oxygen.
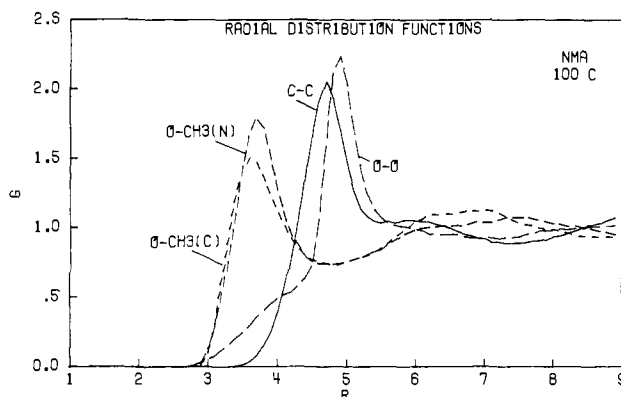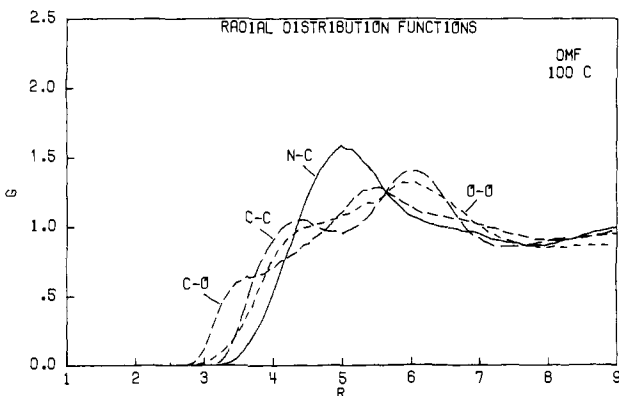

Figure 12. Rdfs for liquid DMF computed with the OPLS functions.

only show that there are an average of four O–H contacts below 2.8 Å. The second peak in the O–H rdfs can also be easily assigned to the hydrogen not hydrogen bonded to the oxygen. This is consistent with open hydrogen bonds as in I and II (Figure 2) rather than bifurcated forms.

Assignments can also be proposed for the two other pronounced double peaks. For the O–O rdf, the two peaks result from the hydrogen bonding to H(C) and H(T). The O–O separation is ca. 1 Å less when the hydrogen bonding is to H(C) rather than H(T). Thus, we can predict that the first peak near 4 Å should mostly disappear for the O–O rdf in NMA. This is confirmed in Figure 9. The twin peaks for the N–N rdf have a similar origin and again the first one is nearly eliminated for NMA (Figure 8).

NMA. The computed rdfs for NMA are shown in Figures 8–10. No diffraction data are available for comparison at this time. Again, hydrogen bonding is clearly reflected in the first peaks in the N–O and O–H rdfs. These peaks integrate to 1.15 and 1.01, respectively. Thus, each monomer may participate in roughly two hydrogen bonds which is fully consistent with the anticipated chain

structure also found in the solid.[22,36]

The other rdfs are less structured than for formamide due to the small (2.3%) concentration of cis hydrogens in NMA. This is apparent in the near vanishing of the first peaks in the N–N and O–O rdfs mentioned above as well as for carbonyl C–C. However, there are still some O–O contacts between 3 and 4 Å in NMA which likely reflect hydrogen bonds to the few cis monomers and alternative geometrical arrangements of near-neighbor trans monomers. One final point from Figures 4 and 10 is that N···H π-type hydrogen bonding must be essentially ruled out for liquid formamide and NMA since the number of contacts below 3 Å is negligible.

DMF. An X-ray study has been reported recently for liquid DMF at 25 °C.[23c] In contrast to formamide, no distinct peaks were found in the total radial distribution curve beyond 3 Å. The conclusion was that liquid DMF is "practically fully disordered".[23c] The individual rdfs in Figures 11–13 obtained from the liquid simulation do show significant structure and require reexamination of the above conclusion. The discrepancy results from the continuous overlap of peaks beyond 3 Å; no peak is substantially
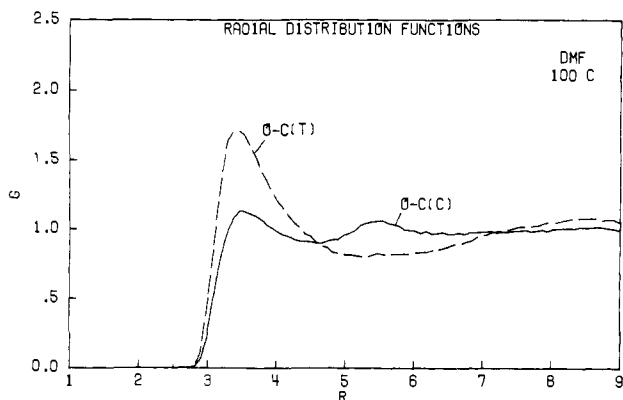
Potential Functions for Amides and Peptides

J. Am. Chem. Soc., Vol. 107, No. 3, 1985 575

Figure 13. O–CH$_3$ rdfs for liquid DMF computed with the OPLS functions.
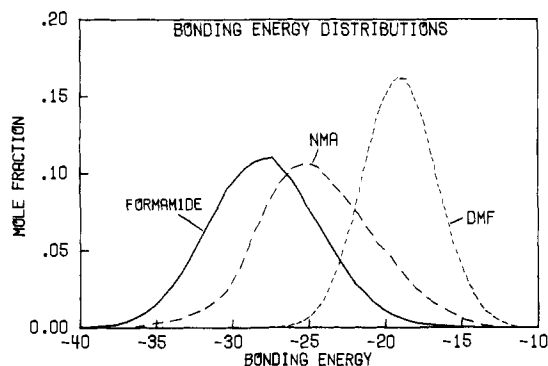

Figure 14. Distributions of total intermolecular bonding energies (kilocalories/mole) for monomers in liquid amides computed with the OPLS functions. The ordinate gives the mole fraction of monomers with the bonding energy on the abscissa. Units for the ordinate are mole fraction per kilocalorie/mole.

higher or well removed from the rest as in the case of the N–O rdfs for formamide and NMA. The peaks are also broader for DMF due to the dominance of general dipole–dipole interactions instead of more geometrically restrictive hydrogen bonding. Clearly, there must be significant local order in DMF in view of its substantial heat of vaporization. This is also apparent in dipole correlation functions presented below.

The N–N rdf in Figure 11 has a classic shape. It is reminiscent of the rdf for liquid argon or the C–C rdf for methane,[20] though the first peak is broader for DMF. It is most similar to the C–C rdf in liquid neopentane.[20] In each of these cases the first peak integrates to 12 neighbors which is the same as for close packing of spheres. Thus, the distribution of nearest neighbors in DMF appears to occur in a roughly spherical shell. Some other insights into the structure of liquid DMF can be obtained from Figure 13. The largest number of short (ca. 3 Å) intermolecular contacts involve oxygen and the methyl groups. Of course, this is reasonable Coulombically. Furthermore, short contacts with oxygen are significantly more common for the trans methyl group. This effect also has an electrostatic origin since the oxygen and trans methyl group are most closely in line with the dipole moment vector for a DMF monomer. There are some relatively short carbonyl carbon–oxygen distances as well (Figure 12) that may result from favorably stacked dimers.

(d) **Energy Distributions.** The energetic environment in the liquids was also monitored during the simulations. The distributions of total intermolecular bonding energies for the monomers are shown in Figure 14. The monomers experience unimodal distributions of energetic environments covering ranges of ca. 15 kcal/mol for DMF and 25 kcal/mol for formamide and NMA. The broader ranges for the latter result from the hydrogen bonding which provides a much wider range of individual dimer interactions. This fact is illustrated in Figure 15 which contains the distributions of dimerization energies for a monomer. These curves have large spikes near 0 kcal/mol due to the many interactions
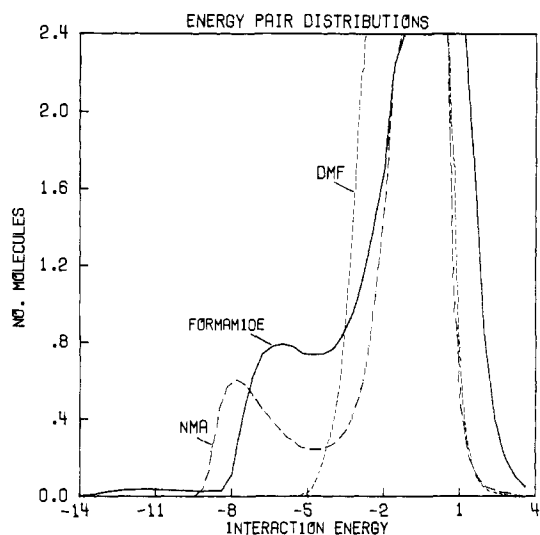

Figure 15. Distributions of dimerization energies (kilocalories/mole) for monomers in liquid amides computed with the OPLS functions. The ordinate records the number of molecules that interact with the reference monomer with the energy on the abscissa. Units for the ordinate are molecules per kilocalorie/mole.

with distant molecules in the bulk, while the interactions at low energy reflect favorable contacts with near neighbors. Hydrogen bonding extends the favorable interactions to –14 kcal/mol for formamide and to –9.2 kcal/mol for NMA (viz. Table II). The dipole–dipole interactions for DMF provide a much narrower distribution with a negligible number of interactions more attractive than –5 kcal/mol.

The energy pair distributions (Figure 15) contain important information on the hydrogen bonding. First, the cyclic hydrogen bonds in formamide are revealed in the small, low-energy band from –14 to –8.4 kcal/mol. This is the only geometrical arrangement that can attain such energies. The second band to roughly –4.5 kcal/mol reflects the single hydrogen bonds plus favorable stacked arrangements. Integration to this point yields the average number of neighbors that have these very favorable interactions with a monomer. The average is 4.23. of which the contribution from cyclic dimers is only 0.16. In the next section, a better average for the number of hydrogen bonds is obtained. This number is 2.5, so only 6% of the hydrogen bonded pairs involve cyclic dimers.

For NMA, the concentration of cis monomers is so low that cyclic hydrogen bonding is not observed. Integration of the energy pair distribution to –4.5 kcal/mol yields 1.80 neighbors which is close to the average number of hydrogen bonds (1.77) obtained below.

(e) **Hydrogen-Bonding Analyses.** The hydrogen bonding in liquid formamide and NMA was analyzed further using configurations saved every 5K during the simulations with the OPLS functions. Thus, 200 configurations were analyzed for each liquid. The first issue is the definition of a hydrogen bond. Though we have favored energetic definitions in the past,[17] geometrical definitions are also possible. For the present systems, a combination of the two seemed most appropriate. A purely energetic definition is conveniently suggested by the location of the minimum in the energy pair distributions near –4.5 kcal/mol (Figure 15). However, for the present systems, these energies may also be achieved through stacked arrangements as in Figure 3 that may not correspond to conventional images of a hydrogen bond. An alternative geometrical definition is readily suggested by the sharp first peaks in the O–H rdfs (Figures 7 and 10). Specifically, the locations of the first minima could be taken as limits for hydrogen bonds, i.e., an O–H separation for a pair of monomers must be less than 2.8 Å for formamide and 3.2 Å for NMA. However, it is very likely that there are some dimers with an O–H distance in this range that may have little net attraction; they could even be repulsive. Consequently, the present analyses were based on both criterions: the interaction energy must be below –4.5

Table V. Results of Hydrogen Bond Analyses[a]

	formamide (25 °C)	NMA (100 °C)
no. of H bonds	2.51	1.77
ϵ(H bond)	−6.39	−7.01
ϵ(Coulomb)	−6.58	−6.06
ϵ(LJ)	0.19	−0.95
θ, deg	130.2	136.4
% in N H Bonds		
$N = 0$	1.1	2.6
$N = 1$	11.8	27.0
$N = 2$	36.0	61.4
$N = 3$	38.2	8.8
$N = 4$	12.1	0.2
$N = 5$	0.8	0.0

[a] ϵ's in kcal/mol. ϵ(H bond) is the average hydrogen bond energy which can be decomposed into Coulomb, ϵ(Coulomb), and Lennard-Jones, ϵ(LJ), terms.
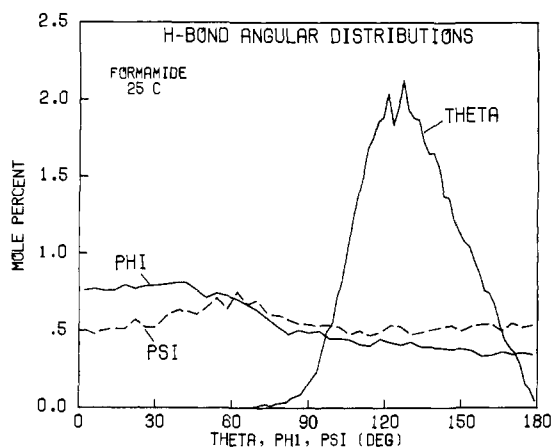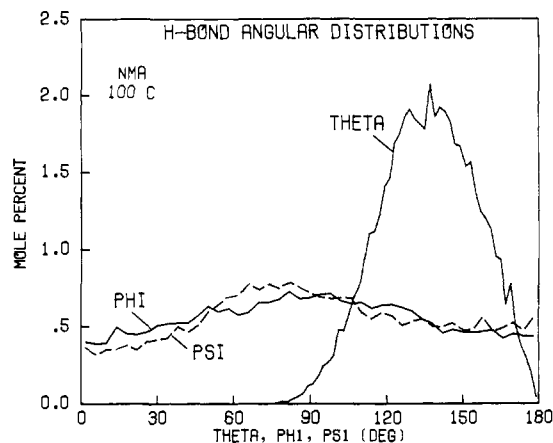

Figure 16. Distributions for hydrogen bond angles in liquid formamide computed with the OPLS functions. θ, ϕ, and ψ are the C=O···H, N—C=O···H, and C=O···H—N angles, respectively. Units for the ordinate are mole percent of hydrogen bonds per degree.

kcal/mol and there must be an O–H distance less than 2.8 Å formamide and 3.2 Å for NMA.

With these definitions, the results in Table V were obtained. Monomers in liquid formamide at 25 °C participate in an average of 2.5 hydrogen bonds. Since only 6% of these involve cyclic dimers (Figure 15), the structure of liquid formamide is overwhelmingly dominated by hydrogen-bonded chains. This finding is in accord with the interpretation of IR, Raman, and ESCA spectra.[21b,c,e] Support is not found for the importance of the cis tetramer proposed by Hinton and Harpool which would require a much higher population of cyclic pairs.[21d,45] The infrequent occurrence of cyclic hydrogen-bonded dimers is illuminating. Although such pairs are strongly favored energetically (Table II), the cyclic geometries are only modestly populated in the configuration space for the liquid. This is most likely a result of the stringent geometrical requirements and correspondingly low entropy for the cyclic form. These observations point out the importance of thermal, configurational averaging for investigating the nature of condensed phases.

Some additional information on the hydrogen bonds in liquid formamide is provided in Table V. The average hydrogen bond strength is −6.39 kcal/mol which can be broken down into Coulomb and Lennard-Jones contributions of −6.58 and +0.19 kcal/mol. The number of hydrogen bonds per monomer ranges from 0 to 5, though 74% of the monomers takes part in two or three hydrogen bonds. In view of the proportion of monomers with more than two hydrogen bonds, the chains in the liquid are highly branched. Angular information was also obtained. The average C=O···H angle, θ, is 130° which is close to the value of 120° derived from a combined X-ray and theoretical analysis.[21f]

Figure 17. Distributions for hydrogen bond angles in liquid NMA as in Figure 16.

The full distribution for θ is presented in Figure 16 and is seen to cover the range from 90° to 180°. Distributions were also obtained for two dihedral angles, the N—C=O···H angle, ϕ, and the C=O···H—N angle, ψ. As demonstrated in Figure 16, there is little preference among the possible values for the dihedral angles; coplanar geometries are not favored as they are in the solid. Clearly, there is great variety among the hydrogen bond geometries in the liquid. Substantial angular flexibility for hydrogen bonds has been noted previously from ab initio calculations on formamide dimers.[46]

For NMA, the calculations reveal 1.8 hydrogen bonds per monomer with an average strength of −7.01 kcal/mol. The Coulombic contribution is now −6.06 kcal/mol, and the Lennard-Jones term is also attractive, −0.95 kcal/mol. The greater strength of the hydrogen bonds for the larger amide results from enhanced Lennard-Jones attraction, offsetting less favorable Coulombic interaction. For NMA, the majority of monomers (61%) participate in two hydrogen bonds. Thus, hydrogen bonded chains dominate the liquid structure, though there is little branching in this case. The occurrence of chains is also consistent with the interpretation of many spectral and dielectric constant measurements on liquid NMA.[22] Some efforts have been made to estimate the average chain length and percentage of unbound NH groups.[22c,d] This is generally fruitless due to the sensitivity to the particular type of measurement and to the rapid variation in predicted chain length as the average number of hydrogen bonds nears 2 ($l = 2/(2 - n_{HB})$).

The angular results for NMA are similar to those for formamide. The average hydrogen bond angle, θ, is 136°. The full distributions for θ, ϕ, and ψ are presented in Figure 17. Smaller values of the dihedral angles are not as common as for formamide due to the steric effect from the methyl group on nitrogen that is cis to oxygen in trans NMA.

(f) Dipole Correlation Functions. In order to address the issue of the degree of structure in liquid DMF, the dipole–dipole correlation function was constructed from the 200 saved configurations. These functions were also computed for formamide and NMA for comparison. Operationally, the cosine of the angle between the dipole vectors for all pairs of monomers was averaged as a function of the distance between the centers of mass of the two molecules. The results are shown in Figure 18. Damped oscillatory behavior is found in each case. The key feature is that at short range (ca. <4.2 Å), the distributions all reveal significant preference for negative values of the cosine of the interdipole angle,

(45) Hinton, J. F.; Harpool, P. D. *J. Am. Chem. Soc.* **1977**, *99*, 349.

(46) Dreyfus, M.; Pullman, A. *Theoret. Chim. Acta* **1970**, *19*, 20. Berthod, H.; Pullman, A. *Chem. Phys. Lett.* **1972**, *14*, 217.

(47) **Note Added in Proof**: In conjuction with other work, a Monte Carlo simulation for liquid DMF at 25 °C and 1 atm has also been carried out. The computed molecular volume (128.1 Å³), density (0.948 g cm⁻³), ΔH_{vap} (11.44 kcal/mol), and C_P (36.1 cal/mol·K) are in close accord with the experimental values[41,42] of 128.6, 0.944, 11.1, and 35.8, respectively. The OPLS functions yield the proper temperature dependence of the density and energy for liquid DMF.
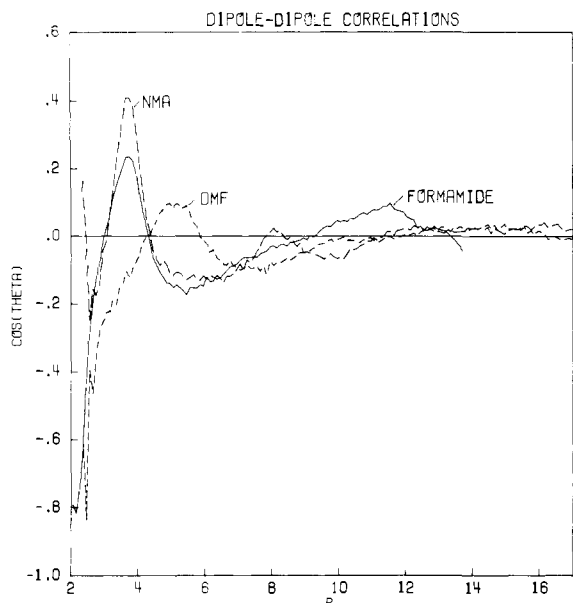
Figure 18. Dipole–dipole correlation functions for liquid amides computed with the OPLS functions. The abscissa records the center-of-mass separation in angstroms.

i.e., antiparallel alignment of neighboring dipoles. This result could be anticipated on electrostatic grounds. In a simple model for a dipolar liquid, one can imagine a linear chain of dipoles arranged end to end: + − + − + −. Attraction with neighboring chains would be optimized if they run in the opposite direction. Extending the idea to three dimensions, one would find that each dipole has the two neighbors in its chain with the dipoles parallel but the torus of nearest dipoles from the neighboring chains would be antiparallel.

The preference for antiparallel alignment of dipoles is substantial at short range in DMF. It may be attributed to some extent to the above type of structuring. It should also be recalled that we found particularly favorable interaction energies for stacked dimers with antiparallel dipoles.

(g) Stereo Plots. To summarize the structural picture of the liquids, stereo plots of the last configurations from the simulations are shown in Figure 19. All 128 monomers are included in each plot. In viewing the plots, the periodicity should be kept in mind so monomers near one face of the cell are also proximate to monomers on the opposite face. The box illustrated in the figures is drawn for clarity a little outside the boundaries of the periodic cube.

In general, local order is discernable, embedded in longer range disorder. Branched hydrogen-bonded chains are ubiquitous for formamide, while cyclic dimers are not clearly apparent. The
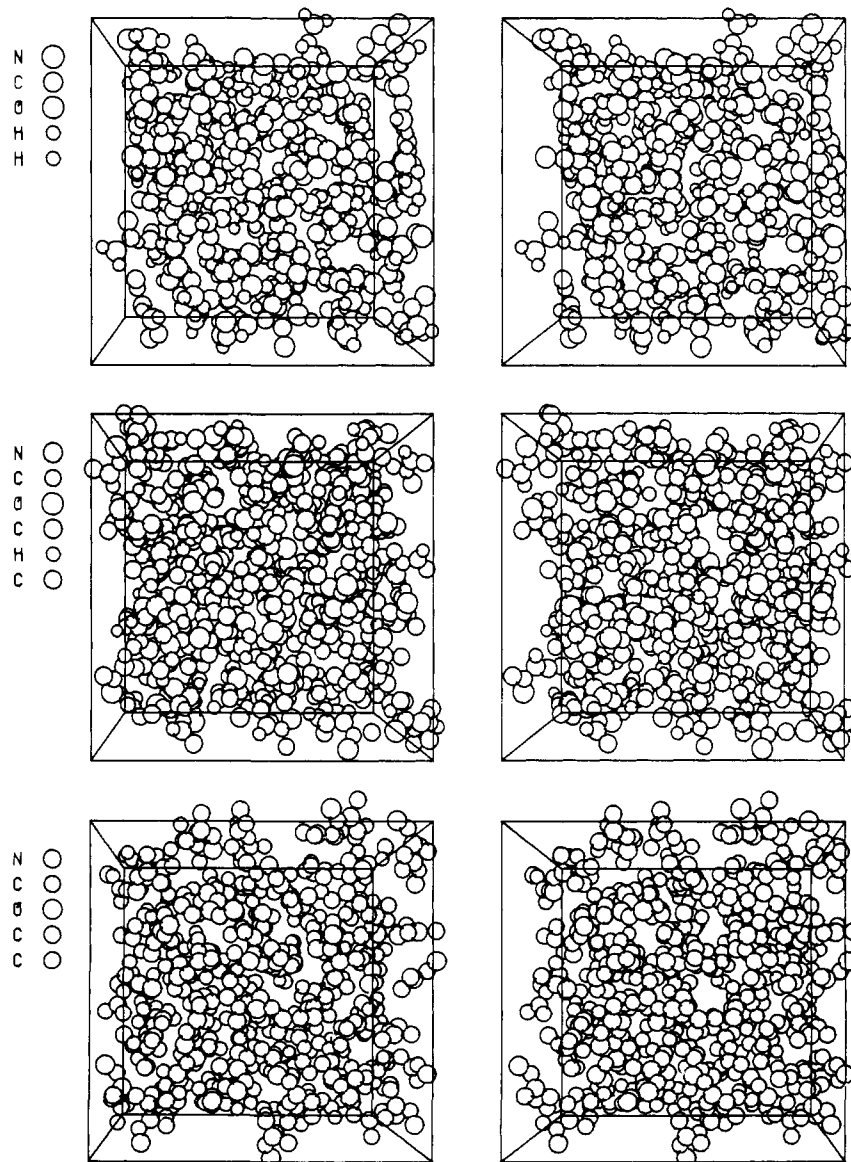

Figure 19. Stereo plots of configurations of liquid (top) formamide, (middle) NMA, and (bottom) DMF.

chains wind wildly and exhibit a broad range of hydrogen bond geometries. There is certainly no preference for coplanar dimers. The same description applies to liquid NMA except that few monomers participate in more than two hydrogen bonds so there is little branching of the chains. Local order is also evident in liquid DMF, although it is not as easy to characterize. Near neighbors definitely organize to provide favorable Coulombic interactions. Short contacts between oxygen and the methyl groups are particularly common. Some neighbors with roughly antiparallel dipoles are apparent. However, this is not a striking feature and seems to be hidden by the apparent medium and long-range disorder.

Conclusion

Optimized intermolecular potential functions have been derived for use in fluid simulations of amides and peptides. The functions have been demonstrated to yield reasonable energetic and structural descriptions of amide dimers and amide–water complexes. Moreover, the principal support for their validity comes from results of Monte Carlo simulations of liquid formamide,

NMA, and DMF. The computed heats of vaporization and densities of the liquids are in essentially exact accord with experimental data. Agreement with available diffraction data on peak positions for radial distribution functions is also excellent. In addition, the simulations yielded thorough descriptions of the structure and hydrogen bonding in the liquid amides. The dominance of hydrogen-bonded chains in liquid formamide and NMA was confirmed, while more subtle local order is apparent in DMF as revealed by dipole correlation functions. The simplicity, form, and demonstrated utility of the OPLS functions make them suitable for study of a wide range of organic and biochemical systems.

How Carbon Monoxide Bonds to Metal Surfaces

Shen-Shu Sung and Roald Hoffmann*

Contribution from the Department of Chemistry, Cornell University, Ithaca, New York 14853. Received May 9, 1984

Abstract: An analysis is presented of the similarities and differences in the bonding of CO to Ni(100), Ni(111), Co(0001), Fe(110), Cr(110), and Ti(0001). The primary interactions in every case are the expected forward and back donation, the mixing of CO 5σ with surface d_{z^2} and s states, and the mixing of CO 2π with metal $d_{xz,yz}$. The latter interaction is dominant. Projections of the density of states and crystal orbital overlap population curves show these interactions clearly. As the metal changes from Ni to Ti, the effects of the rise of the Fermi level and the diffuseness of the d orbitals combine to put more and more electron density into 2π of CO. This is why CO dissociates on the earlier transition-metal surfaces. Our studies of surface coverage show little effect on the diatomic dissociation. There is some indication in the calculations that higher index surfaces should dissociate CO more readily than the lower index ones, but the effect is smaller than that of changing the metal.

The chemisorption of CO on transition-metal surfaces has been the subject of numerous experimental and theoretical studies over the past few decades.[1-6] Brodén, Rhodin, et al. have succeeded in establishing a criterion for dissociative chemisorption behavior of carbon monoxide on a number of transition-metal surfaces as a function of the position of the metal in the periodic table.[1] On the left side of the first-row transition metals, up to Fe, the adsorption is likely to be dissociative. On the right side from Co, it is molecular. Experimental results are available for Ti,[2] Fe,[3] Co,[4] and Ni[1b] in the first row.

In this report we analyze and discuss the electronic consequences of the chemisorption of CO on several transition metals, by using tight binding calculations of the extended Hückel type. Monolayers of CO, CO on Ni(100), comparisons of different metals, different coverages, and different surfaces of the same metal will be studied in this contribution.

Monolayers of CO

The molecular orbitals of an isolated CO molecule are well-known.[7] The highest occupied molecular orbital (HOMO) is mainly a carbon lone pair, as indicated schematically in **1a**.

Its energy (ca. −14 eV)[8] is lower than the d states of transition metals. In the generally accepted end-on CO chemisorption configuration the 5σ is pushed down by surface states, relative to other CO levels. The lowest unoccupied molecular orbital set (LUMO) of the free CO molecule, 2π, consists of two antibonding
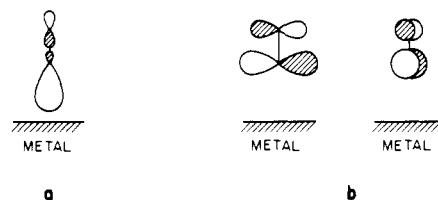
(1) (a) Brodén, G.; Rhodin, T. N.; Brucker, C.; Benbow, R.; Hurych, Z. *Surf. Sci.* **1976**, *59*, 593. (b) Engel, T.; Ertl, G. *Adv. Catal.* **1979**, *28*, 1.

(2) Eastman, D. E. *Solid State Commun.* **1972**, *10*, 933.

(3) Brodén, G.; Gafner, G.; Bonzel, H. *Appl. Phys.* **1977**, *13*, 33; Jensen, E. S.; Rhodin, T. N. *Phys. Rev. B* **1983**, *27*, 3338.

(4) Greuter, F.; Heskett, D.; Plummer, E. W.; Freund, H. J. *Phys. Rev. B* **1983**, *27*, 7117.

(5) (a) Blyholder, G. *J. Phys. Chem.* **1964**, *68*, 2772. (b) Anderson, A. B. *J. Chem. Phys.* **1976**, *64*, 4046. (c) van Santen, R. A. *Proc. Int. Cong. Catal., 8th* **1984**.

(6) Andreoni, W.; Varma, C. M. *Phys. Rev. B* **1981**, *23*, 437. Allison, J. N.; Goddard, W. A., III *Surf. Sci.* **1981**, *110*, L615. Doyen, G.; Ertl, G. *Surf. Sci.* **1977**, *B5*, 641. Doyen, G.; Ertl, G. *Surf. Sci.* **1977**, *69*, 157. Bagus, P. S.; Hermann, K. *Phys. Rev. B.* **1977**, *16*, 4195. Davenport, J. W. *Phys. Rev. Lett.* **1976**, *36*, 945. Bullett, D. W.; Cohen, M. L. *J. Phys.* **1977**, *C10*, 2101.

(7) (a) Jorgensen, W. L.; Salem, L. "The Organic Chemists Book of Orbitals"; Academic Press: New York 1973; p 78. (b) Huo, W. M. *J. Chem. Phys.* **1964**, *43*, 624. McLean, A. D.; Yoshimine, M. *IBM J. Res. Dev. Suppl.* **1968**, *3*, 206.

(8) Gelius, U.; Basiler, E.; Svensson, S.; Bergmark, T.; Siegbahn, K. *J. Electron Spectrosc. Relat. Phenom.* **1973**, *2*, 405. Turner, D.; Baker, C.; Baker A. D.; Brunkle, C. R. "Molecular Photoelectron Spectroscopy"; Wiley-Interscience: New York, 1970